Journal of Analytical and Applied Pyrolysis 173 (2023) 106093

Contents lists available at ScienceDirect

Journal of Analytical and Applied Pyrolysis

journal homepage: www.elsevier.com/locate/jaap

A comprehensive analysis on the synthesis of value-added chemicals via slow pyrolysis: Valorisation of rapeseed residue, whitewood, and seaweed (*Laminaria digitata*)

Fatih Güleç [a,b,*], Hanifrahmawan Sudibyo [c,d], Emily T. Kostas [e], Orla Williams [b], Abby Samson [f], Will Meredith [a], Edward Lester [b]

[a] Low Carbon Energy and Resources Technologies Research Group, Faculty of Engineering, University of Nottingham, Nottingham NG7 2TU, UK
[b] Advanced Materials Research Group, Faculty of Engineering, University of Nottingham, Nottingham NG7 2RD, UK
[c] School of Chemical and Biomolecular Engineering, Energy Systems Institute, Cornell University, Ithaca, NY 14853, USA
[d] Chemical Engineering Department, Universitas Gadjah Mada, Yogyakarta 55281, Indonesia
[e] Advanced Centre of Biochemical Engineering, Bernard Katz Building, University College London, Gower Street, London WC1H 6BT, UK
[f] Department of Mechanical Engineering, University of Sheffield, Sheffield S3 7RD, UK

ARTICLE INFO

Keywords:
Pyrolysis
Biomass
Biofuels
Biorefinery
Bio-chemicals
Reaction Mechanisms

ABSTRACT

Pyrolysis has emerged as a crucial thermochemical conversion technology in the field of biomass processing. Maximising the valorisation of biomass is an essential area of investigation, as it plays a pivotal role in understanding the economic viability and practical application of these advanced technologies. The novelty of this research is to investigate how slow pyrolysis and process interdependencies influence the synthesis of value-added products (bio-oil and biogas formation alongside biochar) from distinctly different UK-based biomass feedstocks: rapeseed residue, whitewood, and seaweed (*Laminaria digitata*). This research also analysed the chemical composition of these products to provide a holistic understanding of the reaction mechanisms involved in their formation. The maximum yield of bio-oil from lignocellulose-rich whitewood was due to the higher selectivity of several endothermic reactions including conversions of 5-hydroxymethylfurfural into cyclic C_5-ketones and alkoxyphenols into cresols and aliphatic hydrocarbons, minimizing the biochar formation. The improvement of bio-oil yield from protein-rich seaweed and lipid-rich rapeseed residue was enabled by the formation of N-heterocyclics (e.g., via the Maillard reaction, Dieckmann cyclization, and Buchwald–Hartwig amination) and aliphatic hydrocarbons (e.g., via deamination of fatty amides and nitriles and decarboxylation of fatty acids), respectively. Meanwhile, the dealkylation and demethoxylation of alkoxyphenols and alkylphenols were responsible for the increased content of hydrocarbons in biogas. The findings provide valuable insights into the maximum valorisation of different types of UK-based biomass resources in slow pyrolysis for the production of biochars and lighter bio-oils to make pyrolysis a key process in biorefineries.

1. Introduction

Valorisation of biomass for producing renewable heat, electricity, and transportation fuels potentially closes the global carbon cycle [1]. A closed carbon cycle is attributed to a process where plants and micro-organisms biogenically capture CO_2 for their growth and development, forming a closed-loop of carbon flow (atmosphere-Earth-atmosphere) without or with minimal carbon losses to the atmosphere [2,3]. The potential near-zero carbon emission to the atmosphere makes biomass a more sustainable source for energy and value-added chemical production [4]. As such, the implementation of biomass-based strategies in the new EU Green Deal (which targets zero carbon emission from energy and speciality chemicals production in order to mitigate climate change), accounts for around half of the proposed renewable resources. [4]. This policy consequently resulted in a substantial increase in biomass demand, increasing the European bioeconomy value which is now worth over €621 billion. In addition, this value represents 4.2% of the EU GDP and allows the employment of 18 million people [5].

* Corresponding author at: Low Carbon Energy and Resources Technologies Research Group, Faculty of Engineering, University of Nottingham, Nottingham NG7 2TU, UK.
E-mail address: Fatih.Gulec1@nottingham.ac.uk (F. Güleç).

https://doi.org/10.1016/j.jaap.2023.106093
Received 31 March 2023; Received in revised form 27 June 2023; Accepted 21 July 2023
Available online 26 July 2023

Biomass can be converted into clean energy and valuable chemicals by a wide range of thermochemical conversion technologies including pyrolysis, hydrothermal processes, gasification, combustion, advanced combustion and chemical looping technologies, and torrefaction [6–20]. Although research and development activities have made significant progress in optimising these technologies, various limitations have emerged due to variability in the physicochemical and biochemical properties of the biomass feedstocks leading to diverse products characteristics over various feedstock and different conversion technologies [21–23], inefficient and not well-integrated biorefineries, poor scalability of the corresponding processes, and a lack of cost-competitive bioproducts [18,24,25]. Thus, maximising the outcome of biomass processing and overcoming the associated challenges greatly relies on adopting an effective thermochemical route. It is essential to carefully choose the most efficient pathway for specific type of biomass while also ensuring that it operates under appropriate conditions that align with the specific goals of the conversion process.

Pyrolysis has emerged as a significant thermochemical conversion technology in biomass processing [26]. A significant number of reviews have been published recently, aiming to better understand the impact of pyrolysis on value-added chemical production [27–31], green hydrogen production [32,33], environment [34,35], prediction via machine learning [31], advanced simulations [36], and techno-economic evaluations [37,38]. Pyrolysis is typically divided into three categories: slow, fast, and flash pyrolysis, differentiated by their heating rates during the process [18]. For a maximum biochar yield, slow pyrolysis using temperatures (ca. 300–700 °C) with a slow heating rate (ca. 0.1–10 °C/min) and long residence times (hours to days) is favoured [39,40]. Fast pyrolysis at intermediate temperatures (ca. 300–700 °C) with higher heating rates (ca. 10–200 °C/s) and short residence times (0.5–10 s) promotes the improvement of bio-oil yield [39,41]. Flash pyrolysis with high temperatures (ca. 900–1300 °C), higher heating rates (>1000 °C/s), and short residence times (<1 s) maximises the gas yield [42]. The solid biochar product can be used in a wide range of applications such as energy production [7], water purification [43], soil amendment [44], CO_2 capture [45], and nanoparticles (for making composites) [46] due to their physicochemical properties [47]. The bio-oil can be extracted for important chemical precursors for the synthesis of value-added chemicals and used for production of transport fuels via cracking (thermal or catalytic cracking) [19,48,49] or anaerobic digestion [50]. The gas product, which may contain syngas, CO_2, and other non-condensable gases, can be used in the Fischer–Tropsch, oxosynthesis, fermentation, isosynthesis, and water-gas-shift (hydrogen/methanol) reactions producing alkanes, alcohols/aldehyde, ethanol, isobutane, and hydrogen/methanol, respectively [51–53]. In addition to primary products of each type of pyrolysis process, it is critical to investigate the value of the outcomes (by products) of the biomass processing, in order to maximise biomass valorisation and minimise biomass processing cost.

While various biomass types have undergone slow pyrolysis to produce biochar, there has been a limited investigation and understanding of the comprehensive valorisation of the outcomes after biochar and potential bio-oil and biogas production. Therefore, the novelty of this research fills this knowledge gap by conducting a comprehensive study to investigate bio-oil and biogas formation alongside biochar production from three distinct UK-based biomass feedstocks, Whitewood, Rapeseed, and L. Digitata, under various slow pyrolysis process conditions. This research also analysed the chemical composition of these products to provide a holistic understanding of the reaction mechanisms involved in their formation. The research combines theoretical chemistry concepts with thermodynamic evaluations of probable reactions to develop reaction pathways and extend the slow pyrolysis applications of these biomass feedstocks. This project's findings provide crucial information towards optimising the use of biomass energy and upcycling waste streams.

2. Material and methods

2.1. Feedstock

Three different biomass feedstocks were used in this study; Whitewood (WW, made from sawdust residues from Northern Ireland, supplied by Wolseley), Brown seaweed *(Laminaria digitata* (LD), UK-sourced marine biomass), and Rapeseed residues (RS, source of agricultural waste, supplied by the School of Biosciences at the University of Nottingham) [3,21,54]. The rape seed (Brassica napus L., variety DK Exalte) was provided by a local farm following the 2017 summer harvest and stored at 20 °C and rH 50% until use) [55,56]. LD was collected at low spring tides in May 2015 near Downderry in Cornwall (UK) (GPS coordinates: 50.3623° N. 4.3687° W) and prepared by following the methods outlined in Ref [54]. These feedstocks are selected as they are all domestically produced in the UK and identifying the best valorisation and potentials value-added products from these feedstocks is significantly important for sustainability, green chemicals, and bioeconomy [54–59].

2.2. Experimental procedures

The slow pyrolysis experiments were investigated in a microactivity test unit, as illustrated in Fig. 1a. Details of the experimental apparatus were presented in our previous publications [57,58,60]. In order to investigate the pyrolysis of these biomass feedstocks, ~5.0 g of WW, RS, LD (having a particle size of 600–850 μm) were placed in a micro-activity reactor, which is located in a preheated (200 °C) tubular furnace. The furnace was then heated to the pyrolysis temperatures, 300, 400, and 550 °C (± 5 °C), with a 20 °C/min of heating rate and then maintained at the pyrolysis temperature for 1.0 h under an inert atmosphere (N_2 with a 12 ml/min of flowrate). Heating rate plays a crucial role in controlling the biochar properties. A slower heating rate (20 °C/min) allows for better control over the thermal decomposition of biomass and can lead to the formation of biochars, which could potentially be applied in energy production thanks to the desirable characteristics, such as higher carbon content, increased stability, and reduced volatiles. Reaction time influences the extent of biomass decomposition and the resulting biochar yield. Longer reaction times allow for more complete decomposition of the biomass, resulting in higher biochar yields. However, excessively long reaction times may lead to undesired secondary reactions, such as excessive volatilisation or thermal degradation of the biochar itself. Although the selection of the heating rate and reaction time is often determined through experimental optimisation, the process conditions in this study were selected to increase the biochar yield and production of lighter oils from the slow pyrolysis of biomass [61]. The pyrolysis products were continuously transferred through a water-ice bath, where the bio-oil samples were condensed and collected. Finally, the uncondensed gas products were collected in a gas sampling bag (1.0 L of capacity). Each set of experiments were carried out in triplicate to assess the reproducibility. Product yield, was calculated using Eqs. 1–2, are presented with error bars indicating the standard deviation [62].

$$\text{Liquid yield } \left(L_{y,Py}, \text{wt.}\%\right) = \frac{m_{liquid}}{m_{Biomass,dry}} * 100 \quad (1)$$

$$\text{Gas yield } \left(G_{y,Py}, \text{wt.}\%\right) = \left(1 - \frac{m_{Liquid} + m_{Char}}{m_{Biomass,dry}}\right) * 100 \quad (2)$$

Where, $m_{Biomass,dry}$ is the dried weight of biomass (g) before pyrolysis, m_{Char} and m_{Liquid} are the dried weight of char and liquid after pyrolysis. The expressions of gas and liquid yields (Eq.1 and Eq.2) do not account for the mass loss during the process.

GC-MS analyses of the generated bio-oils were conducted in full scan mode (*m/z* 40–450) on an Agilent 7890B gas chromatograph interfaced

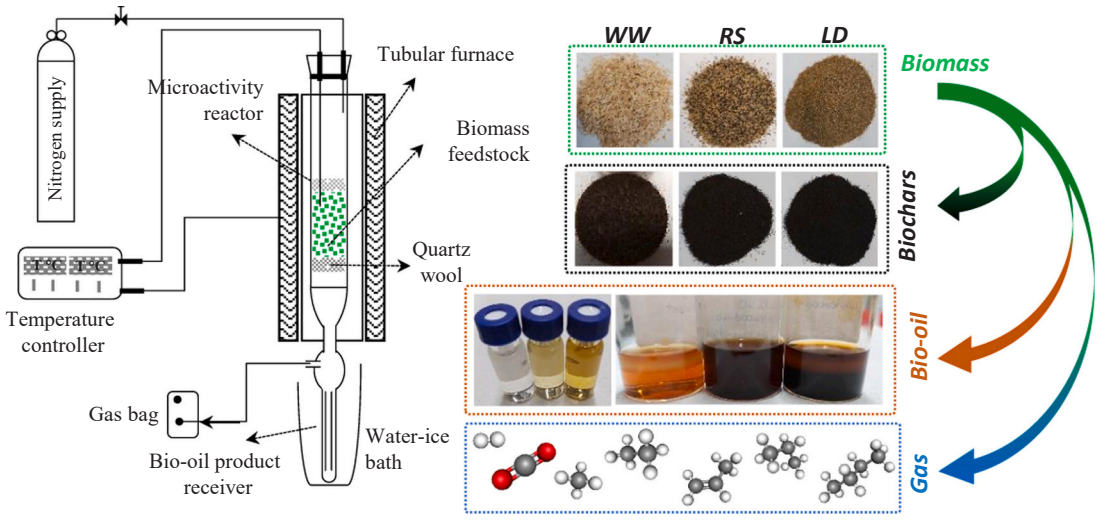

Fig. 1. Process flow diagram of slow-pyrolysis unit (MAT unit).

to a 5977 A ingle quadrupole mass selective detector (MSD) (EI mode, 70 eV). Separation was achieved on a 60 m × 250 μm × 0.25 μm DB-1701 column, with helium as the carrier gas, splitless injection (1 μl), and an oven programme of 50 °C (hold for 2 min) to 300 °C at 5 °C/min, held for 28 min. Compound identification was performed by comparison to the National Institute of Standards and Technology (NIST) library. The gaseous products were immediately analysed after collection in the gas bag using a Clarus 580 GC fitted with an FID and TCD detectors for the hydrocarbon and non-hydrocarbon gases respectively, operating at 200 °C. 5 ml of gas samples were injected (split ratio 10:1) at 250 °C with separation performed on an alumina plot fused silica 30 m × 0.32 mm × 10 μm column, with helium as the carrier gas. The oven temperature was programmed from 60 °C (13 min hold) to 160 °C (10 min hold) at 10 °C/min.

2.3. Feedstock and product characterizations

The proximate analysis (contents of moisture, volatile matter, fixed carbon, and ash) and ultimate analysis (elemental compositions of carbon, hydrogen, and nitrogen) of biomass feedstocks (RS, WW, and LD) and pyrolysis biochars were carried out using a TA-Q500 and LECO CHN 628, respectively. The detailed analysis procedure and conditions are presented in our previous publications [57–59]. The higher heating value (HHV) of feedstocks were measured using a bomb calorimeter (IKA LABORTECHNIK C4000 control) according to BS1016 (Part-5) with benzoic acid as the measurement reference. In order to determine HHV of the biochar, the HHV correlations for each type of biomass feedstock was identified among eleven different HHV correlations presented in previous publications [58,59].

2.4. Identification of pyrolysis mechanisms

Reaction mechanisms occurring during pyrolysis of biomass were identified in order to explain thermochemical phenomena driving the formation of bio-oil, biogas, and biochar with their respective physico-chemical characteristics. To identify the reaction mechanisms, this study utilized the heuristic graph-based approach using a cheminformatic software MØD supported by theoretical chemistry, as well as comprehensive analysis of chemical speciation of the products, similar to the reported method in previous studies [63,64]. In brief, a list of reaction constraints were predefined including (i) type of macromolecules of the feedstocks (reactants) that were decomposed during pyrolysis, (ii) chemical compounds in the bio-oil and biogas detected by chromatography technique, and (iii) the propensity of potential reactions that are well-documented in the chemistry literature. The molecular graph-based approach generated a list of potential molecular structures that may be formed from the pre-determined organic macromolecules and the inputted chromatography-based chemical compounds. These chemical species were connected with each other in order to create a hypothetical reaction network. Finally, each path in the hypothetical reaction network was evaluated according to the Gibbs free energy, which were estimated using eQuilibrator [65], to obtain a thermodynamically-feasible reaction network. The detailed parameter setting for the mechanistic pathway development followed the chemical graph transformation rules in the Double-Pushout approach specified in the literature [66].

3. Results and discussions

3.1. Feedstocks and biochar characterisation

Table 1 shows the proximate and ultimate analysis of raw RS, WW, and LD, and biochars produced by slow pyrolysis of RS, WW and LD at temperature ranges from 250° to 550°C. The characteristics of the biochars produced by pyrolysis of RS, WW, and LD were presented in previous publications [58,59]. The proximate and ultimate analyses of raw biomass feedstocks demonstrated that these feedstocks are three distinctly types. Among them, RS contained the highest carbon content (~56 wt%) compared to WW (~46 wt%) and LD (~30 wt%). Furthermore, RS and WW provided the highest VM (~85 wt%), while it was only ~60 wt% for LD. Regardless of biomass type, pyrolysis enhanced the carbon content while decreasing the hydrogen content in biochar (Table 1) due to the thermal decomposition of hemicellulose and cellulosic compounds. Similarly, increasing the pyrolysis temperature from 300° to 550°C gradually increased the FC and decreased the VM content of biochar, respectively (see Table 1). The FC contents enhanced from ~13 wt% to ~41 wt% for RS, ~13 wt% to ~67 wt% for WW, and ~32 wt% to ~64 wt% for LD at the pyrolysis temperature of 400 °C. In terms of 'energy recovery', the WW biochars derived from pyrolysis at 550 °C provided the highest HHV (38 kJ/g), followed by biochars produced by pyrolysis of RS at 300–400 °C (33.4 kJ/g). However, the ash content significantly increases from ~4 wt% to ~15 wt% for RS and from ~8–21 wt% for LD at the pyrolysis temperature of 400 °C.

An extensive characterisation of these biochars has recently been published [57–59]. Biochars produced via pyrolysis of WW follow dehydration reactions, where the ratio of H/C and O/C were continuously decreased. Similarly, the biochars produced from RS and LD via pyrolysis also showed a dehydration pathway until 400 °C and 300 °C,

Table 1
Characterisation of RS, WW, and LD, and biochars produced by slow pyrolysis.

Biomass and Biochar	Process Conditions	Ultimate analysis (wt%, daf)[a]				Proximate analysis[c,d] (wt%)			HHV[e] (kJ/g)
		C	H	N	O[b]	VM	FC	Ash	
RS-Raw	n.a.	56.1	8.5	2.5	32.9	83.8	12.6	3.7	25.56
RS-PC-300	300 °C, 1 h	69.4	8.7	3.2	18.8	73.4	22.4	4.2	33.48
RS-PC-400	400 °C, 1 h	71.2	7.7	3.5	17.7	48.7	40.9	10.4	33.42
RS-PC-550	550 °C, 1 h	65.9	3.7	4.1	26.4	19.0	66.4	14.6	25.47
WW-Raw	n.a.	46.4	6.6	0.3	46.6	86.3	13.2	0.5	18.94
WW-PC-300	300 °C, 1 h	58.7	6.4	0.3	34.6	66.9	31.2	1.7	24.13
WW-PC-400	400 °C, 1 h	76.1	4.8	0.4	18.7	30.5	67.1	2.3	33.86
WW-PC-550	550 °C, 1 h	-	-	-	-	13.8	83.5	2.6	38.00
LD-Raw	n.a.	29.6	5.3	2.1	63.0	60.2	32.0	8.2	11.73
LD-PC-250	250 °C, 1 h	35.7	4.8	2.8	56.7	45.8	41.5	12.7	13.96
LD-PC-300	300 °C, 1 h	37.6	3.7	3.1	55.6	28.3	55.8	15.9	14.76
LD-PC-400	400 °C, 1 h	34.8	2.9	2.7	59.6	15.3	64.0	20.7	13.55

[a] Dry Ash Free Basis (daf), [b]Oxygen content was determined by difference. [c]VM: Volatile matter, FC: Fixed carbon. [d]Dry basis (db). [e]Higher heating value (HHV). "PC" represents Slow Pyrolysis and the last three digits 300, 400 and 550) represents the process temperature.

respectively. Since at lower temperatures, the primary pyrolysis reactions are typically dominated by the release of volatile compounds (gases and liquids) from the biomass [18]. These volatile compounds are rich in carbon and hydrogen, resulting in a solid residue with a relatively higher carbon content (lower oxygen content) and higher heating value. However, at a higher pyrolysis temperature (550 °C for RS and 400 °C for LD) biochars production carry out through methanation where the ratio of H/C decreases with increasing the ratio of O/C.

As at higher temperatures, secondary reactions become more prevalent. The secondary reactions involve the further breakdown and cracking of the volatile compounds released during primary pyrolysis. The char produced during secondary pyrolysis reactions is relatively rich in carbon but can also contain oxygen-containing functional groups, which arise from the thermal decomposition and oxidation of the original biomass constituents and also has a lower reactivity due to the lack of micropore networks [67]. As a result, the portion of carbon content decreases, and the portion of oxygen content increases in the solid phase products compared to the primary pyrolysis at lower temperatures. Furthermore, the higher pyrolysis temperature leads to more complete volatilisation of carbon and hydrogen, which results in a decreased heating value (higher oxygen-to-carbon ratio) of the solid phase products, as demonstrated in Table 1. The different reaction paths (dehydration and/or demethanation) was attributed to the different thermal decomposition mechanisms of different chemical composition in these biomass feedstocks [59].

3.2. Primary product (biochar, bio-oil, biogas) yields

Fig. 2 shows the yields (bio-oil, biogas, and biochar) for RS, WW and LD pyrolysis at different temperatures. In general, higher reaction temperatures increased the yield of bio-oil and biogas and decreased the yield of biochar. The bio-oil and biogas yields for RS showed an increasing trend from ~17 wt% to ~57 wt% and from ~15 wt% to ~22 wt%, respectively, from 300° to 500°C (Fig. 2a). Biochar yields with RS showed a continuous decrease to ~38 wt% at 400 °C down to ~20 wt% at 550 °C (Fig. 2a), due to the decomposition of cellulose-lignin structures. The pyrolysis of WW also provided similar results with bio-oil and biogas yields increasing from ~28 wt% to ~59 wt% and from ~10 wt% to ~18 wt%, respectively, with increasing temperature from 300° to 550°C (Fig. 2b).

Similar trends were observed for the LD in Fig. 2c. In general, an increase in pyrolysis temperature improved the biogas and bio-oil yields of RS, WW, and LD but decreased the biochar yields due to the thermal decomposition of hemicellulosic (220–315 °C), cellulosic (315–400 °C) and lignin (160–900 °C) structures [10,68,69]. At the same pyrolysis temperature (400 °C), the highest bio-oil yields were observed for WW (~53 wt%) followed by RS (~44 wt%) and then LD (~28 wt%). However, the highest biogas yield was observed for LD (~22 wt%) followed by WW and RS (~18 wt%).

The lower bio-oil yield observed for LD compared to WW and RS can be attributed to the inherent composition and characteristics of LD. LDs typically consist of 46% carbohydrates, 5.5% crude-fibre, 1.0% lipid, 12.9% protein, 26% ash, and 8% moisture [54]. These compositional disparities can significantly impact the pyrolysis process and subsequent bio-oil yield. Since the thermal degradation of carbohydrates and proteins occurs within temperature ranges of 164–497 °C and 209–309 °C [70], respectively. Considering the maximum pyrolysis temperature investigated in this study for LD (400 °C), proteins are decomposed, but a significant portion of carbohydrates may remain unconverted. Conversely, hemicellulose, cellulose, and lignin constitute the primary components of lignocellulosic biomass feedstocks; RS and WW, which decompose within temperature ranges of 220–315 °C, 300–400 °C, and 150–900 °C [13,71], respectively. Considering the maximum pyrolysis temperature investigated for RS and WW (550 °C), a substantial proportion of hemicellulose and cellulose were decomposed, leading to an increased bio-oil yield. Similarly, lignocellulosic biomasses (barley straw) also shows higher biocrude oil yield at 260–320 °C and less than 15 min of residence time using fast hydrothermal liquefaction process [72]. Previous TGA-based slow pyrolysis research on these biomass feedstocks showed a maximum weight loss in the temperature ranges 180–450 °C for RS, 200–370 °C for WW, and 180–330 °C for LD [58,59]. Higher pyrolysis temperatures resulted in further decomposition as a result of the breakdown of the lignin/char structures in these feedstocks [58,59]. Unlike pyrolysis, bio-oil production from a macroalgae (*Enteromorpha clathrate*) was significantly enhanced using two-step hydrothermal liquefaction (HTL) process, where water was used as a solvent [73]. Furthermore, Xu et al. [74] demonstrated that co-pyrolysis of a macroalgae (*Enteromorpha clathrate*) with waste plastics enhanced the biofuel production. The bio-oils produced with this method shows lowered the contents of the acids, oxygenates, and nitrogen-containing compounds, while increased the aromatics and light hydrocarbons contents.

3.3. Bio-oil analysis

Fig. 3 shows the gas chromatograms of the pyrolysis based bio-oil samples produced from RS, WW, and LD. The compounds (each peak) in bio-oils produced by the pyrolysis of RS, WW, and LD at 250–550 °C were identified using retention data and mass spectral database and listed in Table A1, A2, A3, respectively, and shown in Supplementary Appendix A. For all samples the sample amount of feedstock was pyrolyzed and the products were collected in an identical fashion. Prior to analysis the samples diluted in the same amount of solvent (dichloromethane). Therefore, while an internal standard was not employed to

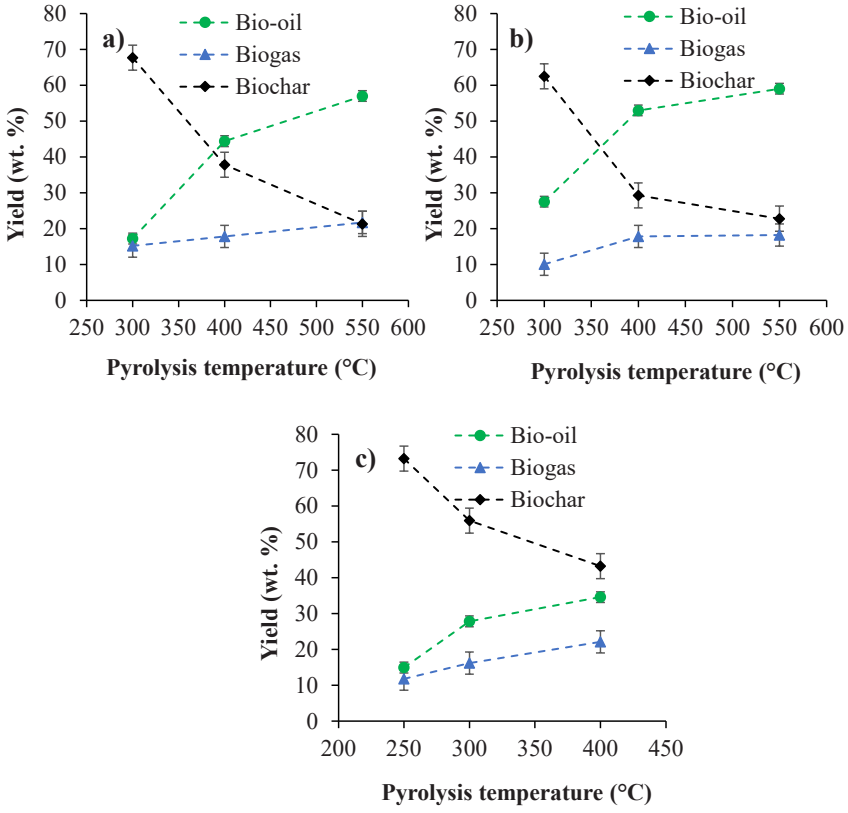

Fig. 2. Bio-oil, Biogas, and Biochar yields from the pyrolysis of the a) RS, b) WW, and c) LD biomass.

allow for absolute quantitation, the relative total peak intensities showed in Table A1-A3 are comparable between the various feedstocks and process temperatures. The peak intensities for the bio-oils produced from RS at 300 °C (Fig. 3a) and LD at 250 °C (Fig. 3c) were relatively low, unlike the bio-oil produced from WW at 300 °C (Fig. 3b). These results indicated that the detected chemical compounds in bio-oil derived from WW has relatively higher concentrations at lower pyrolysis temperatures. The increased concentrations of the detected chemical compounds in bio-oil at higher temperatures were associated with the complete thermal decomposition of biomass organic macromolecules: hemicellulose at 220–315 °C, cellulose at 315–400 °C, and lignin at 160–900 °C [10,68,69]. Moreover, Fig. 3 demonstrates that the molecular size of the detected compounds in the biooil increased with the following order, based on their residence time: LD-bio-oil < WW-bio-oil < RS-bio-oil. Although pyrolysis of different biomass feedstocks resulted in various chemical compositions in bio-oil due to the different feedstocks physicochemical characteristic and thermal decomposition profile, the main peaks for each biomass feedstock all appear to plateau at a specific temperature i.e. RS at 400–550 °C (Fig. 3a), WW at 300–550 °C (Fig. 3b), and LD at 300–400 °C (Fig. 3c).

For the pyrolysis of RS at the low temperature of 300 °C (Table A1), approximately twenty peaks (compounds) were detected and some compounds with the high ratio in the bio-fuel are "2-propanone, 1-(acetyloxy)-", "propanal, 2,2-dimethyl-, oxime" "phenol,2,6-dimethoxy-", "5-*tert*-butylpyrogallol", "2-(4-ethyl-2,5-dimethoxyphenyl)ethanamine", "5,10-diethoxy-2,3,7,8-tetrahydro-1*H*,6*H*-dipyrrolopyrazine". At higher pyrolysis temperatures of 400 °C and 550 °C, approximately 50 compounds were identified. The increase in the pyrolysis temperature not only increased the bio-oil yield, but also increased the number of detected compounds, due to the secondary thermal decomposition of reactive compounds in bio-oil (Table A1).

During the pyrolysis process, the biomass initially underwent primary decomposition resulting in the formation of liquid products (bio-oil) in addition to biochar [75]. This was followed by a secondary decomposition (e.g., cracking and repolymerisation) of unstable intermediates and products in the liquid products into a group of stable liquid and gas compounds [76]. The liquid-phase compounds with the high ratio (percent area) in the bio-oils were mainly "oleanitrile", "8-heptadecene", "9-ctadecenoic acid, methyl ester, (*E*)-", "9-octadecene, 1-methoxy-, (*E*)-", "*trans*-13-octadecenoic acid" "9-octadecenamide, (*Z*)-". While the detected compounds (produced by pyrolysis of RS) at 400 and 550 °C were relatively similar, the detected compounds produced at 300 °C were completely different (see Table A1). This similarity was implicitly demonstrated by the close total peak area of bio-oil's GC-MS chromatogram at 400 and 550 °C (i.e., 65 *10^7 and 112 *10^7 a.u., respectively) and the significantly lower total peak area for 300 °C, i.e., 2 * 10^7 a.u. In addition, the quantity of undefined molecules (smaller peaks) increased with temperature due to the increased formation of low-quantity molecules in the bio-oil mixture, i.e., 15%, 21%, and 26% at 300, 400, and 500 °C, respectively.

Table A2 lists approximately twenty-five peaks (compounds) produced by pyrolysis of WW at different temperatures (300–550 °C). Compared with bio-oils produced by RS (Table A1), most of the chemical compounds in WW-bio-oil were identified, i.e., 91–93% at 300–550 °C (see Table A2). Phenols (e.g., "phenol, 2-methoxy-4-(1-propenyl)-, (*Z*)-", "2-methoxy-4-vinylphenol", "phenol, 2-methoxy-" and "creosol") and furans (e.g., "2-furanmethanol" and "furfural") were the main compounds produced at 300 °C. The increase in the pyrolysis temperature from 300 °C to 400–550 °C only changed the intensity of the detected compounds in WW-bio-oil and maintained relatively similar compositions. The unstable "phenol, 2-methoxy-4-(1-propenyl)-, (*Z*)-" was decomposed into "creosol (2-methoxy-4-methylphenol)", which had the highest intensity in the bio-oil produced at 400–550 °C (Table A2). The increased intensity of "phenol, 2-methoxy-" at 400–550 °C could also be attributed to the decomposition of unstable "phenol, 2-methoxy-4-(1-propenyl)-, (*Z*)-". Likewise, both "furfural" and "2-furanmethanol"

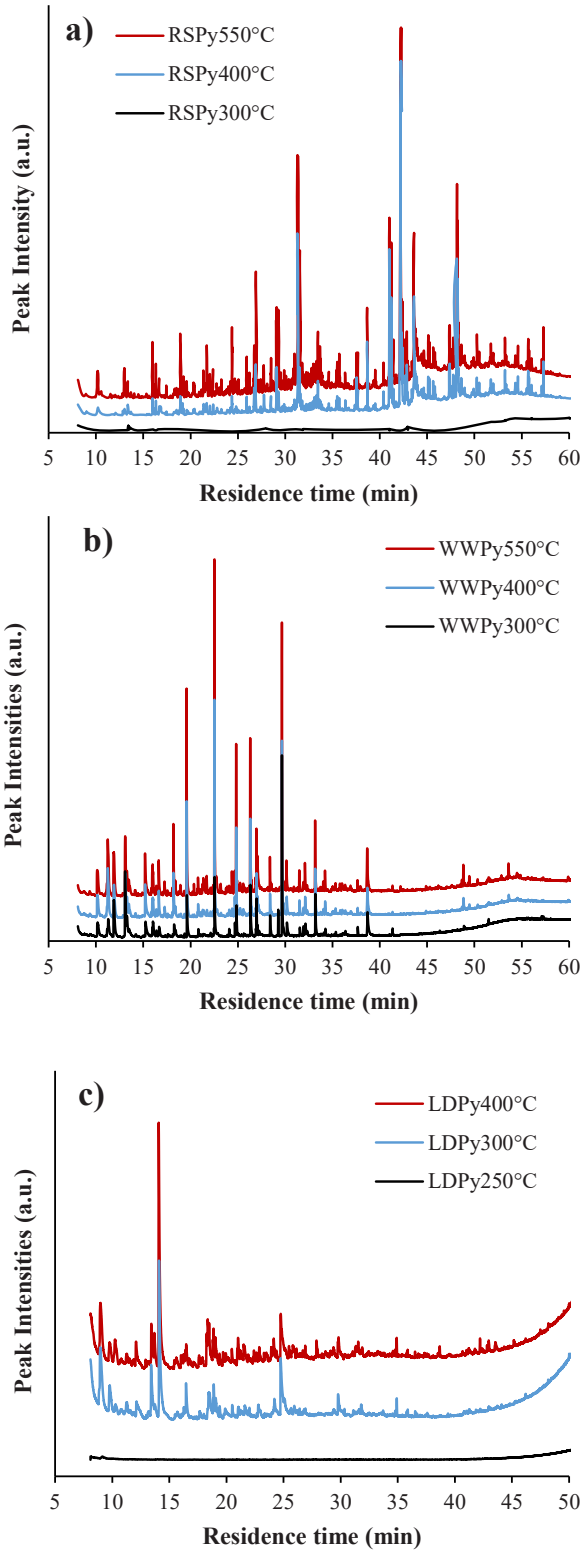

Fig. 3. The total ion current (TIC) chromatograms of GC-MS data obtained from the bio-oil samples produced via pyrolysis of a) RS, b) WW, and c) LD at the temperatures of 250–550 °C (the peak intensities only demonstrate for a temperature compression within the figure not for the comparison of different biomass feedstocks).

intensities decreased with increasing the pyrolysis temperature, which could be attributed to the proportional decrease or decomposition of these products at higher temperatures. Detailed explanations on the reaction mechanisms are given in Section 3.5.

Table A3 lists approximately thirty compounds in the bio-oil produced by pyrolysis of LD at 300 °C. "Ethanone, 1-(2-furanyl)-" had the highest intensity among the detected compounds in bio-oil produced by pyrolysis of LD at 300 and 400 °C. The other compounds with a relatively high ratio in the bio-fuel are "trimethylsilyl cyanide", "geranyl vinyl ether", "3-[*N*-[2-diethylaminoethyl]− 1-cyclopentenylamino] propionitrile", "2-propanone, 1-(acetyloxy)-", "butanoic acid, 4-hydroxy-", and "furan, 3-methyl-". The intensity of these products decreased with increasing pyrolysis temperature from 300 °C to 400 °C, which may be caused by the further thermal cracking or pyrolysis of bio-oils into more stable products (see Section 3.5 for more details).

3.4. Biogas analysis

Fig. 4 shows the gas chromatograms of the hydrocarbon biogas generated by pyrolysis of RS, WW, and LD at 250–550 °C. The gas products of RS pyrolysis were composed of a large amount of light hydrocarbon gases ($C_{1\text{-}2}$: methane, ethane and ethene) and C_3 (propane, propene) and a relatively small amount of C_4 and C_6 hydrocarbon gases. In addition to the hydrocarbon compounds, biogas generated by pyrolysis of these biomasses contained carbon dioxide (CO_2), hydrogen (H_2), carbon monoxide (CO).

Detailed distributions of biogas compounds are given in Fig. 5 and a further detail in each hydrocarbon yield in biogas are provided in Figure B1 in Appendix B. The composition of CO_2, hydrocarbon, and syngas are given in in Figs. 5a, 5c. and 5e, and the distribution of hydrocarbon products from C_1 to C_5 + are illustrated in Figs. 5b, 5d, and 5f. The biogas produced at low temperature pyrolysis (300 °C) predominantly consisted of CO_2 (99.6 wt%) and a relatively low content of hydrocarbon (0.3 wt%) and syngas (0.01 wt%), as shown in Fig. 5a. The increase in pyrolysis temperature from 300° to 550°C enhanced the formation of hydrocarbon gases from 0.3 wt% to 17.4 wt% while reduced the content of CO_2 from 99.6 to 82.1 wt%. Similar results were observed by David and Kopac [77], where the gas generated by the pyrolysis of rapeseed at 500 °C was mainly composed of CO_2 (68.82 wt %), CO, H_2, and hydrocarbons, i.e., C_1 (6.91 wt%) and C_2 to C_7 (<5 wt %). The thermal decomposition of oxygenated compounds (hemicellulose, cellulose, and lignin) produced CO_2 and CO [77,78]. The production of syngas (CO and H_2) was not significantly affected by the pyrolysis temperature, which was atributed to the unstable structure of syngas copounds. Fig. 5b and Fig. 1B-a demonstrate that there was a sequential distribution between hydrocarbon products: (i) C_1 (methane) has the highest portion (~30 wt%, 10.5 mg/g of feedstock) and (ii) hydrocarbon gas with more than one atom of carbon showed an increasing content from C_2 (~23 wt%, 8.11 mg/g of feedstock), C_3 (~19 wt%, 6.98 mg/g of feedstock), C_4 (~12 wt%, 4.47 mg/g of feedstock), and C_5–C_{5+} (~11 wt% 4.11 mg/g of feedstock). While the distribution of hydrocarbons was insignificantly affected by the pyrolysis temeprature (Fig. 5b), the biogas yields and so the production of hydrocarbons (the yield of each hydropcarbons) increased with the pyrolysis temperature (Fig. 2 and Fig. 1B-a).

Fig. 5c shows that WW pyrolysis also provided a biogas having a relatively high CO_2 content (99.4 wt%) with a low content of hydrocarbons (HC) (0.5 wt%) and syngas (0.04 wt%) at 300 °C. The increase in the pyrolysis temperature gradually increased the ratio of HC (14.3 wt %) while decreased the ratio of CO_2 (85.4 wt%) at 550 °C. The distribution of HC, CO_2, and syngas in the biogas produced by WW pyrolysis (Fig. 5c) were relatively similar to the biogas produced by RS pyrolysis (Fig. 5a). However, the distribution of each hydrocarbon compounds in the biogas produced by WW (Fig. 5d) and RS (Fig. 5b) demonstrated differences. Amoung all the HCs, methane has the highest ratio, which is ~42 wt% at 300 °C and gradually increased with the pyrolysis

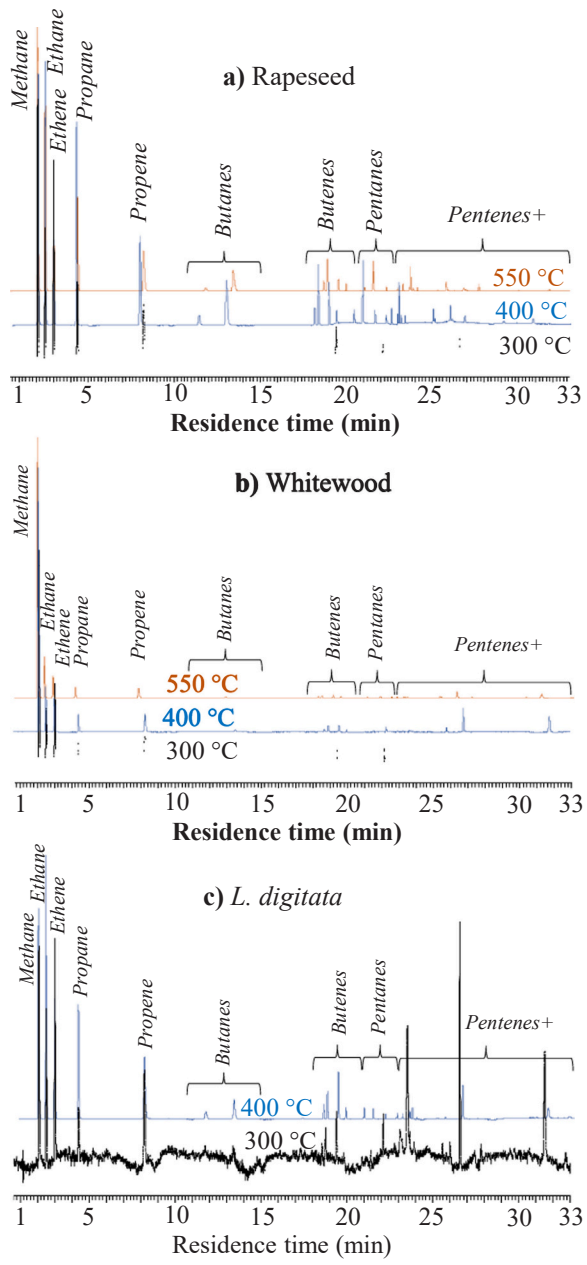

Fig. 4. Gas chromatograms of the biogas produced by pyrolysis of a) RS, b) WW, and c) LD at the temperatures of 300–550 °C.

temperature and reached ~70 wt% at 550 °C. The other HC compounds in biogas accounted for ~15 wt% of C_2, ~7 wt% of C_3, ~3 wt% of C_4, and ~5 wt% of C_5 – C5 + at 550 °C. The biogas produced by WW pyrolysis provided a HC mixture that was rich in methane (70 wt%) and contained a low content of other HC gases (Fig. 5d). Moreover, the biogas produced by RS contained a mixture of hydrocarbons with the respective content decreased with the molecular carbon content (see Fig. 5b) but increase in yield by temperature (see Fig. 2B-b). During the slow pyrolysis process, biogas yield (which also hydrocarbon production) is low but increases at higher temperatures and heating rates [79]. Consistent with these findings, our own research has also demonstrated a similar trend, where higher temperatures lead to increased hydrocarbon gas production, consequently raising the yields of individual hydrocarbons, including hydrogen.

Fig. 5e shows that the biogas produced by LD provided a relatively high CO_2 content (99.8 wt%) at 300 °C. Increasing the pyrolysis temperature did not significantly enhance the production of HC (only ~1.3 wt% at 400 °C Fig. 5e) although the gas yield increased with pyrolysis temperature (Fig. 2). Compare with other feedstocks (i.e., WW and RS), LD provided a relatively higher CO_2 yield by the thermal decomposition via pyrolysis, which was atttributed to the high oxygen content of LD (~63 wt% as presented in Table 1). In addition, the HC distribution in Fig. 5f demonstrated that pyrolysis of LD at 300–400 °C produced a specific HC gas group from methane to pentanes. Higher temperatures resulted in the formation of alkanes and alkenes, while lower temperature (300 C) generated biogas containing mostly alkenes and C_5 + hydrocarbons. Hence, higher pyrolysis temperatue from 300 to 400 C increased and decreased the yield of alkanes and alkenes in the gas-phase product, respectively.

3.5. Pyrolysis mechanisms

This section is structured into three parts. Each part represents mechanistic explanations for pyrolysis of whitewood (WW), seaweed (*Laminaria digitata*, LD), and rapeseed residue (RS), respectively. The first part, Section 3.5.1, begins with pyrolysis pathways of WW because it contains the simplest primary organic macromolecules: lignin and cellulose. In Section 3.5.2, we describe the reaction mechanisms for pyrolysis of LD whose major organic constituents are slightly more complex with the presence of protein in addition to lignin and polysaccharides. Specifically, we describe the reaction pathways that involve the decomposition products of protein (e.g., amino acids and amines) with several precursors derived from the breakdown of lignin and cellulose explained in Section 3.5.1. The last part, Section 3.5.3, discusses the conversion pathways of pyrolysis of RS that contains lignin, polysaccharides, protein, and lipid. This section emphasizes on the formation of chemical compounds derived from lipid degradation products since the previous two sections have covered the mechanisms for the other three organic macromolecules. The overall pyrolysis reaction mechanisms are shown in Fig. 6. Each reaction pathway in Fig. 6 is labelled using *R#*, where *R* represents the initial of any of the organic macromolecules (i.e., C for cellulose/carbohydrates, L for lignin, P for protein, and T for triglycerides) and # is the reaction number. This reaction number is referred in the following sections to allow readers to identify the course of pyrolysis of different reactants at various temperatures. The detected compounds by GC-MS are given in Table A1-A3.

3.5.1. Whitewood (WW)

Bio-oil produced during the pyrolysis of WW was highly associated with the formation of (1) lignin-derived alkoxyphenols and benzaldehydes and (2) cellulose-derived anhydrous sugars, furans, and cyclic C_5-ketones (see Table A2), where as the recovery of biochar was associated with the formation of HMF or furans. Alkoxyphenols (e.g., (*Z*)− 2-methoxy-4-(1-propenyl)-phenol, 4-ethyl-2-methoxy-phenol, and 2-methoxy-4-vinylphenol) were formed via homolytic cleavage (L1) of the β–O–4 and α–O–4 ether motifs attached to the lignin aromatic structure followed by an *ipso* rearrangement [80].

Alkoxyphenols can be converted into benzaldehydes (e.g., 3-hydroxy-4-methoxy-benzaldehyde) through hydrogen abstraction (L3) of one of the methoxyphenol's –OH group[81]. The formation of anhydrous sugars and furans (e.g., furaldehydes and furanic ketones) require the glycosidic bond of cellulose to be homolytically cleaved (C1–C3) to form an intermediate with C═C bond and reducing sugars [9].

The intermediate with C═C bond was converted into levoglucosan via hydrogen transfer (C1) followed by further dehydration and isomerization reactions (C2) to form anhydrous sugars (e.g., 1,6:2,3-dianhydro-4-O-acetyl-β-D-gulopyranose), as shown in Table A2 [82]. Meanwhile, reducing sugars, such as glucose, were tautomerized (C4) into fructose via ring-opening prior to dehydrative cyclization (C5) into 5-hydroxymethylfurfural (HMF) [83]. Subsequently, HMF may evolve through (1) repolymerization producing biochar and (2) elimination of hydroxymethyl group to form furfural, whose aldehyde group may be reduced into hydroxyl group, yielding furfuryl alcohol, e.g.,

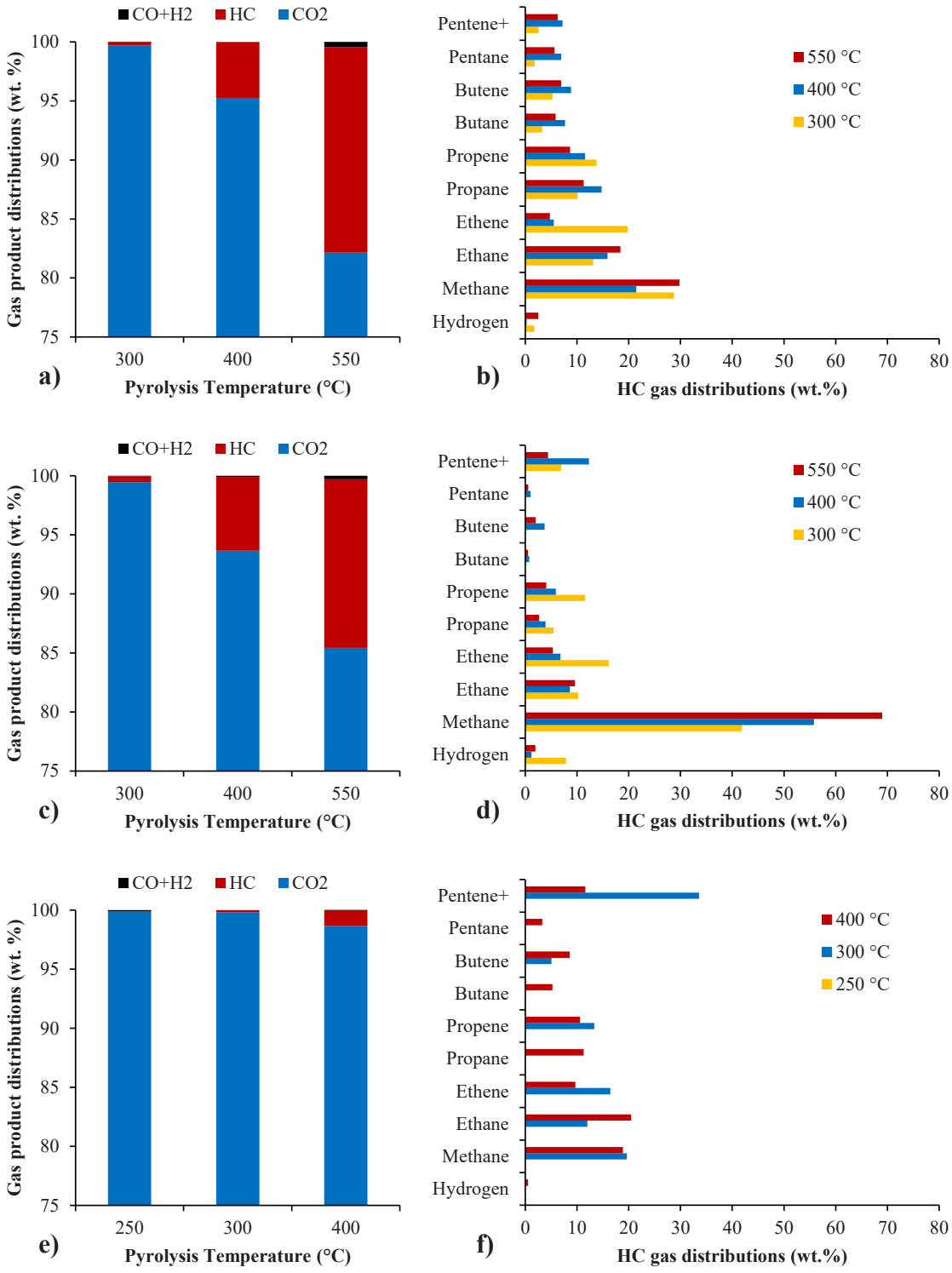

Fig. 5. Gas product distrubution (a, c, e) and hydrocarbon (HC) product distribution (b, d, f) of the biogas produced by pyrolysis of RS (a, b), WW (c, d) and LD (e, f) at 250–550 °C (hydrocarbon gas product yields are provided in Fig. B1 in Appendix B).

2-furanmethanol [84]. Alternatively, furfuryl alcohol may also be obtained via direct decarbonylation of HMF (C6) [85]. Furfuryl alcohol was a precursor for the production of cyclic C_5-ketones (e.g., 3-methylcyclopentane-1,2-dione) via the Piancatelli rearrangement (C8) [86]. The higher bio-oil yield at higher temperatures was associated with the enhanced formation of alkylphenols (i.e., cresols), cyclic C_5-ketones, and aliphatic diketones in addition to the relatively stabilized formation of alkoxyphenols, furans, and benzaldehydes. At higher temperatures, HMF conversion into cyclic C5-ketones were favored over recondensation into biochar. Moreover, higher temperatures may convert alkoxyphenols in bio-oil into alkylphenols (L6) through two demethylation pathways and one demethoxylation pathway. The first demethylation pathway included the generation of hydroxyphenols (e.g., catechol or resorcinol, L14) as intermediates followed by intramolecular hydrogen

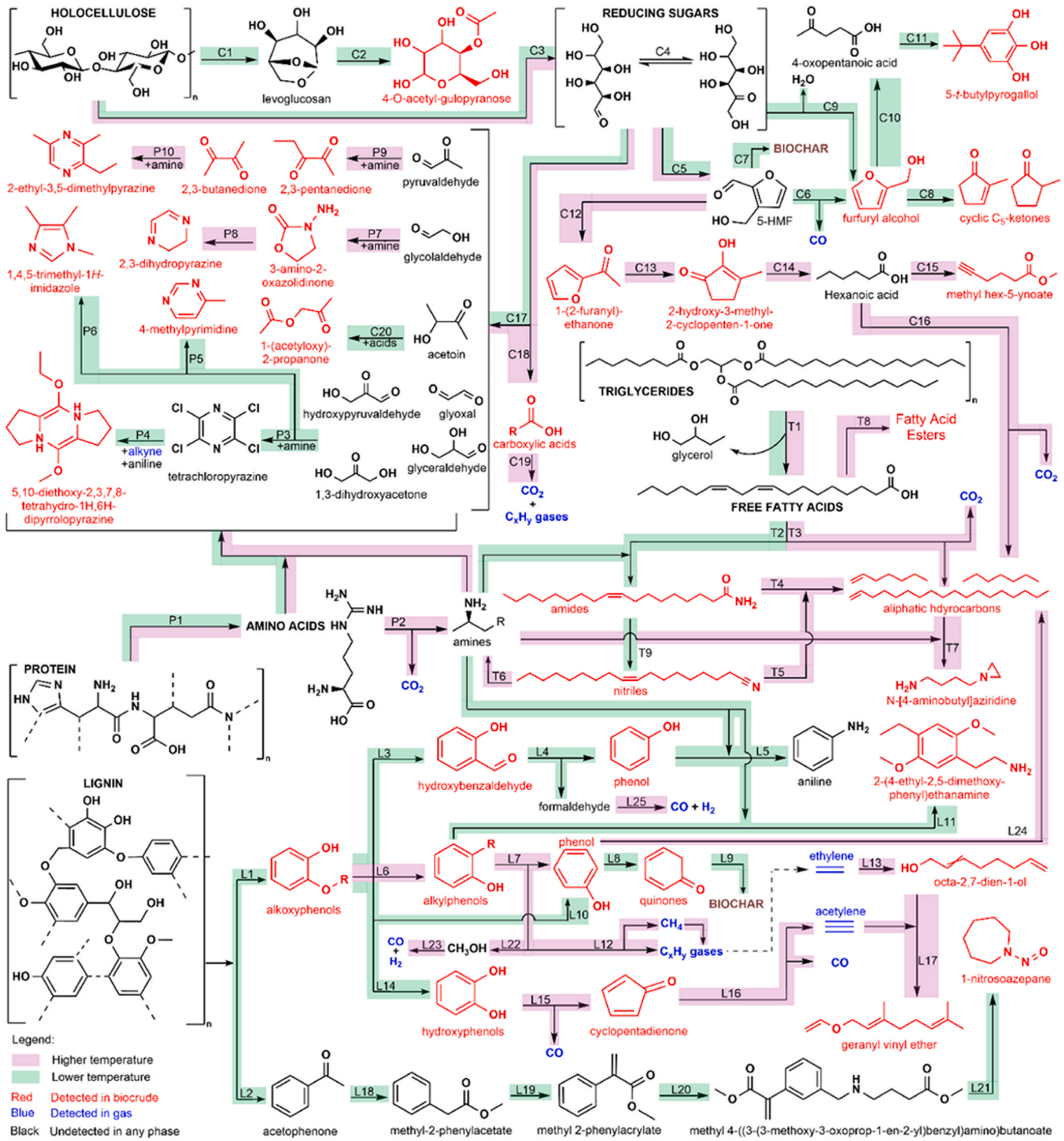

Fig. 6. Proposed mechanisms for the slow pyrolysis of RS, WW, and LD at 250–550 °C. Each reaction pathway in Fig. 6 is labelled using *R#*, where *R* represents the initial of any of the organic macromolecules (i.e., C for cellulose/carbohydrates, L for lignin, P for protein, and T for triglycerides) and # is the reaction number. Red and blue colour shows detected molecules in bio-oil and biogas, respectively, and black colour indicates the undetected compounds in any product phase. The green and red colours highlighting the reaction arrow indicate the lower and higher pyrolysis temperature that are favorable for the formation of specific intermediates and products.

abstraction at the alkyl group by phenoxy radical and 1,2-aryl migration, leading to producing quinone methide [87]. The quinone methide was readily hydrogenated into *o*-cresol. Noteworthy is that quinones are susceptible to recondensation into biochar (L9) [88]. Therefore, higher reaction temperatures and adequate hydrogen donor were necessary in order to give a high selectivity of the hydrogenation step. Hydrogen donation occur, in situ, via various reactions including the decomposition of alcohols (L23) and formaldehyde (L25) [88,89].

The second demethylation pathway involves an *ortho* replacement of the alkyl group by hydrogen radicals, yielding *m*-cresol [90]. In addition to the cresols detected in the bio-oil (see Table A2), the demethylation pathway was confirmed by the increased generation of methane gas at

higher temperatures, as shown in Fig. 5d. Methane was formed by hydrogen donation towards methyl radicals released during demethylation (L12). In addition, the formation of other hydrocarbons may follow due to the potential methane polymerization [91], as illustrated in Fig. 5. Meanwhile, the demethoxylation pathway was more straightforward, directly forming methanol and alkylphenols (L7) products (L22) [92]. This pathway was confirmed by the higher content of syngas, the decomposition products of methanol (L23), in the final biogas product (see Fig. 5c).

While the enhanced formation of cyclic C_5-ketones in bio-oil at higher temperatures was expected due to the endothermic properties of Piancatelli rearrangement [86], the formation of aliphatic diketones indicated that the products of retro-aldol condensation of glucose (C17) and the amino acids in WW (e.g., phenylalanine) were more reactive. The retro-aldol reaction products, such as pyruvaldehyde and glyceraldehyde, may undergo nucleophilic interaction with α-carbons of amino acids (aldol condensation), followed by amino acid-mediated decarboxylation (P9) generating 2,3-pentanedione [93,94]. In addition, 2,3-butanedione may be derived from amino acid-mediated chain elongation of pyruvaldehyde. Another key intermediate derived from retro-aldol reaction product was glycolaldehyde, which may be converted into oxazoles (e.g., 3-amino-2-oxazolidinone, see Table A2) via intramolecular cyclization (P7) of Schiff bases with the carboxylic moiety of the amino acid [95].

3.5.2. Seaweed (Laminaria digitata, LD)

The characteristic composition of bio-oil (Table A3) from pyrolysis of LD was the significant content of N-heterocyclics due to high protein content in the feedstock, i.e., alkyl-substituted pyrazines and imidazoles, aziridines, and azepines. The pyrazines and imidazoles were formed via the Maillard reaction involving α-dicarbonyls/α-hydroxycarbonyls and amino acids [96]. Specifically, the presence of alkyl substituents demonstrated that the carbonyl compounds must include 2,3-pentanedione and 2,3-butanedione, which originated from the amino acid-mediated decarboxylation and chain elongation (P9) of glyceraldehyde and pyruvaldehyde [97]. Aziridines (e.g., *N*-[4-aminobutyl] aziridine) were formed via oxidative coupling (T7) of aliphatic hydrocarbons (i.e., products of alkoxyphenols dealkylation and fatty acid decarboxylation) with primary amines derived from decarboxylation of amino acids [98]. Meanwhile, the precursors for the formation of azepines (e.g., hexahydro-1-nitroso-1*H*-azepine) were methyl 2-phenylacetate and benzylamine. Methyl phenylacetate reacted with formaldehyde forming methyl 2-phenylacrylate, which underwent amination (L20) with benzylamine and alkylation to form amino-α,ω-diester [99]. Accelerated Dieckmann cyclization rate through Thorpe-Ingold interactions while reducing retro-Michael-derived by-products produced the *t*-butoxy carbamates, which were decarboxylated into azepines (L21) [100].

In addition to N-heterocyclics, the content of furanic ketones, cyclotenes (i.e., hydroxymethyl-substituted cyclopentenones), aliphatic esters and ethers, and alkylphenols in bio-oil were also significantly improved at higher temperatures. Similarly, phenolic compounds increased at high temperature compared with those at the low-temperature hydrothermal liquefaction of seaweed (*Enteromorpha clathrate*)[73]. The formation of furanic ketones, cyclotenes, and aliphatic esters occurred through a set of sequential reaction steps. Cellulose in LD was initially converted into HMF following the same mechanisms as pyrolysis of WW, i.e., C3–C5. Subsequently, HMF may undergo dehydration and rearrangement (C12) into furanic ketones, e.g., 1-(2-furanyl)ethanone [101]. Further Piancatelli rearrangement of 1-(2-furanyl)ethanone resulted in the formation of cyclotenes (C13), which were susceptible to aromatic ring opening into hexanoic acid (C14) [102]. Due to its high reactivity towards hydrogenation and esterification (i.e., reaction with methanol derived from demethoxylation of alkoxyphenols), hexanoic acid was converted into methyl hex-5-ynoate (C15). Meanwhile, aliphatic ethers, particularly geranyl vinyl ether, was formed from the Favorski-Reppe vinylation involving 1,8-octanediol and acetylene [103]. 1,8-octanediol was obtained from oligomerization of ethylene (i.e., a product of dealkylation of alkoxyphenols) followed by oxidation. Acetylene was obtained from decomposition of cyclopentandienolyl radical (L16), which were products of catechol radical decomposition (L15) [90].

3.5.3. Rapeseed residue (RS)

Pyrolysis derived bio-oil from RS (Table A1) at lower temperatures contained mostly cyclic ketones, alkoxy- and dihydroxy-phenols, N-heterocyclics, and keto-ethers. The formation of ketones and alkoxyphenols followed the same reaction pathways of cellulose and lignin decomposition as pyrolysis of WW (see Section 3.5.1). The formation of dihydroxyphenols (e.g., 5-tert-butylpyrogallol) was attributed to further derivation of furfural via Diels-Alder, fragmentation, and oligomerization reactions (C10–C11). The formation of N-heterocyclics followed the Maillard reaction (P3 and P5) and the Buchwald–Hartwig amination (P4) [95,104]. The former produced six-membered N-heterocyclics, such as 4-methylpyrimidine, 2-piperidinemethanamine, and 2,3,5,6-tetrachloropyrazine. The latter produced pyrrolopyrazines (e.g., 5,10-diethoxy-2,3,7,8-tetrahydro-1*H*,6*H*-dipyrrolo[1,2-a:1′,2′-*d*]pyrazine) through the reaction between dialkynes with anilines, the amination products of phenols (L5). The dialkyne precursors were obtained from the Sonogashira cross-coupling of alkynes (i.e., decomposition products of cyclopentandienolyl radical, L16) with 2,3,5,6-tetrachloropyrazine. Meanwhile, the formation of keto-ethers was enabled by keto-enol tautomerization of acetoin (i.e., a retro-aldol condensation product of glucose, C17) forming keto-alcohols. Keto-alcohols were reactive with acids forming acetoxyketones (C20), e.g., 1-(acetyloxy)- 2-propanone [105].

At higher temperatures, the bio-oil was predominantly free fatty acids, amides, nitriles, and short- and long-chain aliphatic hydrocarbons with significantly low content of phenols. This result indicated that reactions breaking down lipid or triglycerides in RS were activated at higher temperatures. Triglycerides may undergo hydrolysis (T1), yielding free fatty acids and glycerol [106]. Subsequently, free fatty acids may be derived into fatty acid esters (e.g., methyl (*E*)− 9-octadecenoate) via esterification with methanol (T8), fatty amides (e.g., (*Z*)− 9-octadecenamide) via amidation with amino acids/amines (T2), fatty nitriles (e.g., oleonitrile) via dehydration of fatty amides (T9), and aliphatic hydrocarbons (e.g., hexadecane, heptadecane, and octadecane) via direct decarboxylation of fatty acids (T3) [107–109]. Likewise, deamination of fatty amides (T4) and nitriles (T5) and produced similar aliphatic hydrocarbon structures [110]. The low content of phenols in biocrude was due to the enhancement of a series of dealkylation and ring-opening of alkoxyphenols and alkylphenols, which increasingly produced hydrocarbon gases and aromatic benzenes and aliphatic hydrocarbons in bio-oil. The enhanced formation of benzenes was predicted to be a cause of reduced biochar yield at higher temperatures. The aromatic π-electrons (H-bond acceptor) of benzenes may form hydrogen bond with the –OH group of cellulose-derived intermediates (e.g., α-dicarbonyls/α-hydroxycarbonyls) yielding more thermochemically -stable compounds in bio-oil, which were resistant to repolymerization into biochar [88,90].

4. Conclusions

In this study, the production of bio-oil and biogas from RS, WW, and LD via slow pyrolysis were comprehensively investigated and the value-added compounds (chemicals) were identified as part of the project of "Optimisation of Integrated Bioenergy and High Value Product Processing Pathways for UK Biomass Resources". This is novel research that reports a comprehensive comparative study on the investigation of bioenergy potential of three distinctly different biomass feedstocks; rapeseed residue, whitewood, and seaweed (Laminaria Digitata), via slow pyrolysis.

- Regardless of biomass feedstocks, slow pyrolysis enhanced bio-oil and biogas yields while decreasing the biochar yields. At the same process conditions (400 °C), WW provides the highest bio-oil yields (~53 wt%) followed by RS (~44 wt%) and LD (~34 wt%). On the other side, LD provides the highest biochar yield (~43 wt%) followed by RS (~38 wt%) and WW (~29 wt%).
- Among the biochars, WW biochars and RS biochars produced at 400 °C provided relatively high HHV (~33 kJ/g) while LD biochars provide relatively low HHV (~14 kJ/g).
- As for the bio-oil products, pyrolysis of RS results in larger molecules compared to WW and LD. The increase in the pyrolysis temperature increases the number of compounds due to the secondary thermal decomposition of unstable compounds in bio-oils. The main compound produced by slow pyrolysis of RS, WW, and LD are "*Oleanitrile*", phenols (mainly "*Creosol*"), and furfurals (mainly "*Ethanone, 1-(2-furanyl)-*"), respectively.
- Biogas samples predominantly consist of CO_2 regardless of biomass feedstocks and process temperature. However, pyrolysis of RS and WW (at higher temperatures) increase the ratio of hydrocarbons and deacrease the ratio of CO_2 in the biogas mixture.

The maximum yield of bio-oil from lignocellulose-rich whitewood was due to the higher selectivity of several endothermic reactions including conversions of 5-hydroxymethylfurfural into cyclic C5-ketones and alkoxyphenols into cresols and aliphatic hydrocarbons, minimising the biochar formation.

Results in this study has helped to inform reaction mechanisms and the corresponding process conditions that could allow the maximization of the pyrolysis products value as basis for making pyrolysis a key process in biomass biorefineries. This study and the previous studies [57–59] comprehensively demonstrates how the optimal holistic biomass processing pathways and process interdependencies are influenced by feedstocks (RS, WW, and LD) and process conditions.

CRediT authorship contribution statement

Fatih Güleç: Conceptualization, Methodology, Formal analysis, Investigation, Validation, Visualization, Writing - original draft, Writing - review & editing. **Hanifrahmawan Sudibyo:** Methodology, Formal analysis, Investigation, Visualization, Writing - original draft, Writing - review & editing. **Emily T. Kostas:** Methodology, Funding acquisition, Writing - review & editing. **Orla Williams:** Conceptualization, Funding acquisition, Methodology, Supervision, Writing - review & editing. **Abby Samson:** Methodology, Funding acquisition, Writing - review & editing. **Will Meredith**: Conceptualization, Methodology, Writing - review & editing. **Edward Lester:** Conceptualization, Methodology, Supervision, Project administration, Funding acquisition, Writing - review & editing.

Declaration of Competing Interest

The authors declare that they have no known competing financial interests or personal relationships that could have appeared to influence the work reported in this paper.

Data Availability

Data will be made available on request.

Acknowledgement

This research was funded and supported by the EPSRC, BBSRC and UK Supergen Bioenergy Hub [Grant number EP/S000771/1], the University of Nottingham Anne McLaren Research Fellowship (Dr Orla Williams), and the UK Biotechnology and Biological Sciences Research Council (BBSRC) Discovery Fellowship (Dr Emily Kostas) [Grant number BB/S010610/1]. We also would like to acknowledge Dr David Gray, Dr Filippo Bramante, and Dr Vincenzo Di Bari for supplying the Rapeseed for this project.

Appendix A. Supporting information

Supplementary data associated with this article can be found in the online version at doi:10.1016/j.jaap.2023.106093.

References

[1] P. Shrivastava, P. Khongphakdi, A. Palamanit, A. Kumar, P. Tekasakul, Biomass-.-. Convers. Biorefinery (2020) 1.
[2] M. Kumar, A.O. Oyedun, A. Kumar, Renew. Sustain. Energy Rev. 81 (2018) 1742.
[3] E.T. Kostas, O.S. Williams, G. Duran-Jimenez, A.J. Tapper, M. Cooper, R. Meehan, J.P. Robinson, Biomass-.-. Bioenergy 125 (2019) 41.
[4] S.P. Andersen, B. Allen, G.C. Domingo, , Inst. Eur. Environ. Policy (IEEP) (2021).
[5] E. Comission, in, Office of the European Union Brussels, Belgium (2018).
[6] P.J. Arauzo, M. Atienza-Martínez, J. Ábrego, M.P. Olszewski, Z. Cao, A. Kruse, Energies 13 (2020) 4164.
[7] F. Fan, X. Xing, S. Shi, X. Zhang, X. Zhang, Y. Li, Y. Xing, Trans. Chin. Soc. Agric. Eng. 32 (2016) 219.
[8] E.T. Kostas, G. Durán-Jiménez, B.J. Shepherd, W. Meredith, L.A. Stevens, O. S. Williams, G.J. Lye, J.P. Robinson, Chem. Eng. J. 387 (2020), 123404.
[9] S. Wang, G. Dai, H. Yang, Z. Luo, Prog. Energy Combust. Sci. 62 (2017) 33.
[10] H. Yang, R. Yan, H. Chen, D.H. Lee, C. Zheng, Fuel 86 (2007) 1781.
[11] N. Abdoulmoumine, S. Adhikari, A. Kulkarni, S. Chattanathan, Appl. Energy 155 (2015) 294.
[12] L. Cao, K. Iris, X. Xiong, D.C. Tsang, S. Zhang, J.H. Clark, C. Hu, Y.H. Ng, J. Shang, Y.S. Ok, Environ. Res. 186 (2020), 109547.
[13] F. Güleç, L.M.G. Riesco, O. Williams, E.T. Kostas, A. Samson, E. Lester, Fuel 302 (2021), 121166.
[14] Y. Shen, Biomass-.-. Bioenergy 134 (2020).
[15] R.V.P. Antero, A.C.F. Alves, S.B. de Oliveira, S.A. Ojala, S.S. Brum, J. Clean. Prod. 252 (2020).
[16] M. Wilk, A. Magdziarz, K. Jayaraman, M. Szymańska-Chargot, I. Gökalp, Biomass-.-. Bioenergy 120 (2019) 166.
[17] R. Sharma, K. Jasrotia, N. Singh, P. Ghosh, S. srivastava, N.R. Sharma, J. Singh, R. Kanwar, A. Kumar, Chem. Afr. 3 (2019) 1.
[18] F. Güleç, E.H. Şimşek, H.T. Sarı, Chem. Eng. Technol. 45 (2022) 167.
[19] F. Güleç, W. Meredith, C.-G. Sun, C.E. Snape, Fuel 244 (2019) 140.
[20] F. Güleç, W. Meredith, C.-G. Sun, C.E. Snape, Energy 173 (2019) 658.
[21] O. Williams, G. Newbolt, C. Eastwick, S. Kingman, D. Giddings, S. Lormor, E. Lester, Appl. Energy 182 (2016) 219.
[22] O. Williams, C. Eastwick, S. Kingman, D. Giddings, S. Lormor, E. Lester, Fuel 158 (2015) 379.
[23] S.V. Vassilev, C.G. Vassileva, V.S. Vassilev, Fuel 158 (2015) 330.
[24] F.H. Isikgor, C.R. Becer, Polym. Chem. 6 (2015) 4497.
[25] M. Guo, W. Song, N. Biotechnol. 49 (2019) 48.
[26] D. Shen, R. Xiao, S. Gu, H. Zhang, Cellul. -Biomass-.-. Convers. (2013) 193.
[27] A.N. Amenaghawon, C.L. Anyalewechi, C.O. Okieimen, H.S. Kusuma, Environ., Dev. Sustain. (2021) 1.
[28] P. Li, K. Wan, H. Chen, F. Zheng, Z. Zhang, B. Niu, Y. Zhang, D. Long, Catalysts 12 (2022) 1067.
[29] O.A. Qamar, F. Jamil, M. Hussain, H. Ala'a, A. Inayat, A. Waris, P. Akhter, Y.-K. Park, Chem. Eng. J. 454 (2023), 140240.
[30] J.A. Okolie, E.I. Epelle, M.E. Tabat, U. Orivri, A.N. Amenaghawon, P.U. Okoye, B. Gunes, Process Saf. Environ. Prot. 159 (2022) 323.
[31] J.A. Okolie, D. Awotoye, M.E. Tabat, P.U. Okoye, E.I. Epelle, C.C. Ogbaga, F. Güleç, B. Oboirien, Iscience (2023).
[32] A.K. Vuppaladadiyam, S.S.V. Vuppaladadiyam, A. Awasthi, A. Sahoo, S. Rehman, K.K. Pant, S. Murugavelh, Q. Huang, E. Anthony, P. Fennel, Bioresour. Technol. (2022), 128087.
[33] G. Lopez, L. Santamaria, A. Lemonidou, S. Zhang, C. Wu, A.T. Sipra, N. Gao, Nat. Rev. Methods Prim. 2 (2022) 20.
[34] H. Chen, R. Shan, F. Zhao, J. Gu, Y. Zhang, H. Yuan, Y. Chen, Chem. Eng. J. 451 (2023), 138979.
[35] D. Gahane, D. Biswal, S.A. Mandavgane, BioEnergy Res. 15 (2022) 1387.
[36] H. Luo, X. Wang, X. Liu, X. Wu, X. Shi, Q. Xiong, J. Anal. Appl. Pyrolysis 162 (2022), 105433.
[37] A. Inayat, A. Ahmed, R. Tariq, A. Waris, F. Jamil, S.F. Ahmed, C. Ghenai, Y.-K. Park, Front. Energy Res. 9 (2022) 993.
[38] M. Tripathi, J.N. Sahu, P. Ganesan, Renew. Sustain. Energy Rev. 55 (2016) 467.
[39] P. Basu, Biomass gasification, pyrolysis and torrefaction: practical design and theory, Academic press,, 2018 (p).
[40] H. Tan, C. Lee, P. Ong, K. Wong, C. Bong, C. Li and Y. Gao, A review on the comparison between slow pyrolysis and fast pyrolysis on the quality of lignocellulosic and lignin-based biochar, at: IOP Conference Series: Materials Science and Engineering, 012075.
[41] H. Sudibyo, M. Pecchi, H. Harwood, M. Khare, S. Karunwi, G. Tan, J.W. Tester, Ind. Eng. Chem. Res. (2022).
[42] L. Li, J.S. Rowbotham, C.H. Greenwell and P.W. Dyer, in, Elsevier, 2013.

[43] W. Hao, E. Björkman, M. Lilliestråle, N. Hedin, Ind. Eng. Chem. Res. 53 (2014) 15389.
[44] R. Subedi, C. Kammann, S. Pelisseti, D. Sacco, C. Grignani and S. Monaco, Recycling of organic residues for agriculture: from waste management to ecosystem services, at: 15th International Conference RAMIRAN,
[45] Y. Guangzhi, Y. Jinyu, Y. Yuhua, T. Zhihong, Y. DengGuang, Y. Junhe, RSC Adv. 7 (2017) 4152.
[46] Z. Liu, F. Zhang, S.K. Hoekman, T. Liu, C. Gai, N. Peng, ACS Sustain. Chem. Eng. 4 (2016) 3261.
[47] M.-M. Titirici, M. Antonietti, N. Baccile, Green. Chem. 10 (2008) 1204.
[48] F. Güleç, W. Meredith, C.-G. Sun, C.E. Snape, Chem. Eng. J. 389 (2020), 124492.
[49] F. Güleç, Demonstrating the applicability of chemical looping combustion for fluid catalytic cracking unit as a novel CO2 capture technology, University of Nottingham, Chemical Engineering, 2020,
[50] M. Zamri, S. Hasmady, A. Akhiar, F. Ideris, A. Shamsuddin, M. Mofijur, I. R. Fattah, T. Mahlia, Renew. Sustain. Energy Rev. 137 (2021), 110637.
[51] J. Street, F. Yu, Biofuels 2 (2011) 677.
[52] K. Melin, M. Hurme, Cellul. Chem. Technol. 44 (2010) 117.
[53] P. Nkulikiyinka, Y. Yan, F. Güleç, V. Manovic, P.T. Clough, Energy AI 2 (2020), 100037.
[54] E.T. Kostas, D.A. White, D.J. Cook, Algal Res. 28 (2017) 211.
[55] S. De Chirico, V. di Bari, M.J.R. Guzmán, C.V. Nikiforidis, T. Foster, D. Gray, Food Chem. 316 (2020), 126355.
[56] S. De Chirico, V. di Bari, T. Foster, D. Gray, Food Chem. 241 (2018) 419.
[57] F. Güleç, O. Williams, E.T. Kostas, A. Samson, L.A. Stevens, E. Lester, Fuel 330 (2022), 125428.
[58] F. Güleç, O. Williams, E.T. Kostas, A. Samson, E. Lester, Energy Convers. Manag. 270 (2022), 116260.
[59] F. Güleç, A. Samson, O. Williams, E.T. Kostas, E. Lester, Fuel Process. Technol. 239 (2022), 107492.
[60] F. Güleç, W. Meredith, C.E. Snape, J. Energy Inst. (2023), 101187.
[61] S.H. Russell, J.L. Turrion-Gomez, W. Meredith, P. Langston, C.E. Snape, J. Anal. Appl. Pyrolysis 124 (2017) 536.
[62] J. Koechermann, K. Goersch, B. Wirth, J. Muehlenberg, M. Klemm, J. Environ. Chem. Eng. 6 (2018) 5481.
[63] H. Sudibyo, J.W. Tester, Sustain. Energy Fuels 6 (2022) 5474.
[64] J.L. Andersen, C. Flamm, D. Merkle, P.F. Stadler, IEEE/ACM Trans. Comput. Biol. Bioinforma. 16 (2017) 510.
[65] M.E. Beber, M.G. Gollub, D. Mozaffari, K.M. Shebek, A.I. Flamholz, R. Milo, E. Noor, Nucleic Acids Res. 50 (2022) D603.
[66] J.L. Andersen, C. Flamm, D. Merkle, P.F. Stadler, MATCH Commun. Math. Comput. Chem. 80 (2018) 45.
[67] D. Mohan, C.U. Pittman Jr, P.H. Steele, Energy fuels 20 (2006) 848.
[68] E. Lester, M. Gong, A. Thompson, J. Anal. Appl. Pyrolysis 80 (2007) 111.
[69] M. Carrier, L. Auret, A. Bridgwater, J.H. Knoetze, Energy Fuels 30 (2016) 7834.
[70] W.-H. Chen, Y.-S. Chu, J.-L. Liu, J.-S. Chang, Energy Convers. Manag. 160 (2018) 209.
[71] C.L. Waters, R.R. Janupala, R.G. Mallinson, L.L. Lobban, J. Anal. Appl. Pyrolysis 126 (2017) 380.
[72] Z. Zhu, X. Guo, L. Rosendahl, S.S. Toor, S. Zhang, Z. Sun, S. Lu, J. Zhao, J. Yang, G. Chen, Biomass-.-. Bioenergy 165 (2022), 106587.
[73] S. Wang, S. Zhao, X. Cheng, L. Qian, B. Barati, X. Gong, B. Cao, C. Yuan, Bioresour. Technol. 319 (2021), 124176.
[74] S. Xu, B. Cao, B.B. Uzoejinwa, E.A. Odey, S. Wang, H. Shang, C. Li, Y. Hu, Q. Wang, J.N. Nwakaire, Process Saf. Environ. Prot. 137 (2020) 34.
[75] W.-J. Liu, H. Jiang, H.-Q. Yu, Chem. Rev. 115 (2015) 12251.
[76] A.K. Varma, L.S. Thakur, R. Shankar, P. Mondal, Waste Manag. 89 (2019) 224.
[77] E. David, J. Kopac, J. Anal. Appl. Pyrolysis 134 (2018) 495.
[78] B.B. Uzun, A.E. Pütün, E. Pütün, J. Anal. Appl. Pyrolysis 79 (2007) 147.
[79] M. Asadullah, M.A. Rahman, M.M. Ali, M. Rahman, M. Motin, M. Sultan, M. Alam, Fuel 86 (2007) 2514.
[80] H. Kawamoto, J. Wood Sci. 63 (2017) 117.
[81] M. Asmadi, H. Kawamoto, S. Saka, J. Anal. Appl. Pyrolysis 92 (2011) 88.
[82] Y.-C. Lin, J. Cho, G.A. Tompsett, P.R. Westmoreland, G.W. Huber, J. Phys. Chem. C. 113 (2009) 20097.
[83] M. Wang, C. Liu, X. Xu, Q. Li, J. Anal. Appl. Pyrolysis 120 (2016) 464.
[84] S. Wang, X. Guo, T. Liang, Y. Zhou, Z. Luo, Bioresour. Technol. 104 (2012) 722.
[85] H. Sudibyo, M. Pecchi, J.W. Tester, Sustain. Energy Fuels 6 (2022) 2314.
[86] T. Shen, R. Hu, C. Zhu, M. Li, W. Zhuang, C. Tang, H. Ying, RSC Adv. 8 (2018) 37993.
[87] E. Dorrestijn, P. Mulder, J. Chem. Soc., Perkin Trans. 2 (1999) 777.
[88] W. Schutyser, aT. Renders, S. Van den Bosch, S.-F. Koelewijn, G. Beckham, B. F. Sels, Chem. Soc. Rev. 47 (2018) 852.
[89] X. Ouyang, X. Huang, Y. Zhu, X. Qiu, Energy Fuels 29 (2015) 5835.
[90] M. Asmadi, H. Kawamoto, S. Saka, J. Anal. Appl. Pyrolysis 92 (2011) 76.
[91] A. Serovaiskii, V. Kutcherov, Sci. Rep. 10 (2020) 1.
[92] M. Ishikawa, M. Tamura, Y. Nakagawa, K. Tomishige, Appl. Catal. B: Environ. 182 (2016) 193.
[93] V.A. Yaylayan, A. Keyhani, J. Agric. Food Chem. 47 (1999) 3280.
[94] Z. Srokol, A.-G. Bouche, A. Van Estrik, R.C. Strik, T. Maschmeyer, J.A. Peters, Carbohydr. Res. 339 (2004) 1717.
[95] H. Xing, V. Yaylayan, Eur. Food Res. Technol. 247 (2021) 1095.
[96] A. Wnorowski, V.A. Yaylayan, J. Agric. Food Chem. 48 (2000) 3549.
[97] P.V. Guerra, V.A. Yaylayan, J. Agric. Food Chem. 60 (2012) 11440.
[98] D.E. Holst, D.J. Wang, M.J. Kim, I.A. Guzei, Z.K. Wickens, Nature 596 (2021) 74.
[99] S.A. Sharif, E.D. Calder, Fb.G. Delolo, A. Sutherland, J. Org. Chem. 81 (2016) 6697.
[100] S.M. Sakya, A.C. Flick, J.W. Coe, D.L. Gray, S. Liang, F. Ferri, M. Van Den Berg, K. Pouwer, Tetrahedron Lett. 53 (2012) 723.
[101] Q. Wu, B. Zhao, S. Liu, S. Yu, L. Huang, A.J. Ragauskas, Catal. Sci. Technol. 10 (2020) 3423.
[102] R. Tressl, B. Helak, E. Kersten, D. Rewicki, J. Agric. Food Chem. 41 (1993) 547.
[103] R. Matake, Y. Adachi, H. Matsubara, Green. Chem. 18 (2016) 2614.
[104] R. Heckershoff, T. Schnitzer, T. Diederich, L. Eberle, P. Krämer, F. Rominger, M. Rudolph, A.S.K. Hashmi, J. Am. Chem. Soc. (2022).
[105] M. Weerawatanakorn, J.-C. Wu, M.-H. Pan, C.-T. Ho, J. Food Drug Anal. 23 (2015) 176.
[106] X. Wang, L. Sheng, X. Yang, Bioresour. Technol. 229 (2017) 119.
[107] H. Sudibyo, R. Rochmadi, M. Fahrurrozi, Eng. J. 21 (2017) 45.
[108] S. Chiaberge, I. Leonardis, T. Fiorani, G. Bianchi, P. Cesti, A. Bosetti, M. Crucianelli, S. Reale, F. De Angelis, Energy fuels 27 (2013) 5287.
[109] S.A. Shipilovskikh, V.Y. Vaganov, E.I. Denisova, A.E. Rubtsov, A.V. Malkov, Org. Lett. 20 (2018) 728.
[110] G.H. Prado, Y. Rao, A. de Klerk, Energy Fuels 31 (2017) 14.